Optoelectronic Performance of Vertical Cavity Surface Emitting InGaAs/InP QW Laser in non-conventional orientation

Sourav Roy[1, 2,*], Md. Imtiaz Kabir[1], K.M Abdullah Al-Mamun[1]
[1]Department of Electrical and Electronic Engineering, JUST, Jessore-7408, Bangladesh
[2]Department of Electrical and Electronic Engineering, KUET, Khulna-9203, Bangladesh
[*] E-mail: souravroy2k9@gmail.com

***Abstract*—Here, the optoelectronic performance of lattice matched InGaAs/InP vertical cavity surface emitting LASER is numerically simulated using MATLAB in (100), (110), (111), (113) and (131) crystal orientation by solving an eight-band *k.p* Hamiltonian using finite difference scheme including spin-orbit coupling. Tensor plane rotation formulae is applied to change the wave-vector k and Hamiltonian from orthodox (100) plane orientation. It is shown that there is a notable interrelationship between optical emission spectra and crystal plane orientations. The highest and lowest gains are estimated in (111) and (100) orientations with their respective peak emission wavelengths of 1770nm and 1680 nm at the carrier injection density of 2.5×10^{18} cm^{-3}. The outcome of this paper would be a stimulus to design ultra-speed optoelectronic devices with performance amelioration by using non-100 oriented epitaxial layers.**

Keywords—VCSEL; Lattice matching; k.p method; Crystal orientation; Optical gain

I. INTRODUCTION

Time division multiplexing (TDM) systems operating beyond 40 Gbit/s, combined with wavelength division multiplexing (WDM), promise auspicious solutions for over-Tbit/s systems due to elevation in lightwave communications technology and the research interest is now towards 100-Gbit/s-class architecture. One of the major barricade in realizing such ultrahigh speed TDM design is the upgradation of ultrahigh speed electronic ICs [1]. Vertical cavity surface emitting laser (VCSEL) first revealed in 1992 (optical pumping) and 1993 (electrical pumping) at Sandia National Laboratories and Chiao Tung University in Taiwan [2-3] is a strong contender for high power laser source. The larger output aperture of VCSELs produces a lower divergence angle of the output beam, and makes possible high coupling efficiency with optical fibers. Mirrors having high reflectivity, in contrast to most edge-emitting lasers, reduce the threshold current of VCSELs, resulting in low power consumption. The oldest and probably the most utilized hetero-structure laser technique is AlGaAs/GaAs QW. However, the InP-based lattice matched systems InP/$In_{0.53}Ga_{0.47}As$,came into attention not only because of its material affinity with the optical devices, but also due to its superior drift-diffusion properties with respect to the AlGaAs QW systems. At the InP/InGaAs interface, the higher valence band discontinuity as compared to that in the conduction band (ΔE_C= 0.25eVand ΔE_V=0.34eV) provides a high injection efficiency. Moreover, the typical electron mobility is about double that of GaAs and the ohmic contact resistance to n-InGaAs is lower than GaAs due to the lower Schottky barrier height and higher saturation doping density of donors. The emission wavelength from this laser system ranges from 1.2 to 1.7 μm which covers low dispersion and minimum attenuation region in present-day optic-fiber communication (OFC) [4].

Recently, it has become established that energy band dispersion profile of III-V materials is strongly interrelated with crystal orientations. While better crystalline film quality is achieved for (100) oriented growth of QWs, the internal quantum efficiency reduces with increasing wavelength, resulting partially from the decreased oscillator strength due to the field injected separation of electrons and holes [5]. Performance amelioration in optoelectronic devices can be realized in nonconventional orientation having favorable band structure due to anisotropy of the topmost bulk valence band and minimum interaction between hole sub-bands. Advanced film preparation techniques such as molecular beam epitaxy (MBE) and metal-organic chemical vapor deposition (MOCVD) enables the growth of non- (100)-orientated crystal structure [6-7]. In our previous works, the influence of crystal orientation on different optoelectronic properties of InGaAs/GaAs QW has been studied [8]. There are few reports on orientation-dependent growth of InGaAs/InP QW [9-10]. However, to best of our knowledge, the optical emission profile of InP based laser in non-conventional orientation and its possible application in 1.55 μm OFC is unavailable.

Throughout this paper, the optical properties of lattice matched ZB InP/$In_{0.53}Ga_{0.47}As$ VCSEL laser have been demonstrated by using the 8*8 k.p matrix for (100), (110), (111), (113) and (131) crystal orientations. Here, 10 nm quantum well is sandwiched between 7 nm barrier layers. To reveal the optoelectronic properties in (hkl) crystal orientations, plane transformation matrixes are used to modify the wave vector and Hamiltonian matrix from orthodox (100) crystal orientation. The wave functions and Eigen energies of the proposed architecture are evaluated using the numerical finite difference method. The emission profile is anticipated using the energy dispersion profile and wave functions.

The description of this paper is designed as follows: the theoretical formula to calculate optical properties of the InGaAs/InP QW are mentioned in section 2. Results and discussions on the energy band structure and optical emission spectra are illustrated in section 3. Finally, a summary is depicted in section 4.

II. THEORY

A. LASER Structure:

In Laser structure of Fig. 1, a 10nm $In_{0.53}Ga_{0.47}As$ active layer is sandwiched between 7nm InP barrier layers and high band gap GaInAsP is used as cladding layer. Two $Al_{0.05}Ga_{0.42}In_{0.53}As$/ InP DBRs of mean reflectivity 99.5% are also used as mirrors. All the layers are grown on GaAs

978-1-5090-6122-8/16/$31.00 ©2016 IEEE

substrate. In non-orthodox (hkl)-orientated laser structure; the h, k and l parameters in the active region is changed.

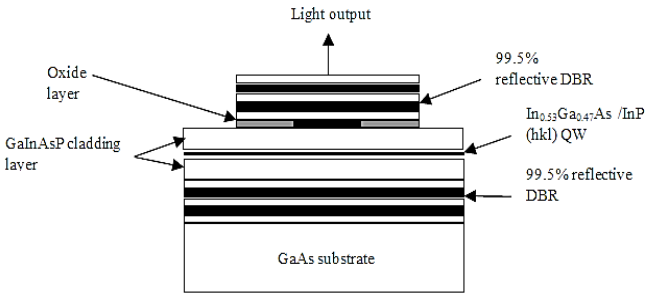

Fig. 1: Structure of lattice matched InGaAs/InP VCSEL

B. *The k.p Method of Band-Structure Calculation near Γ-point:*

The electronic energy band profile is solved in the envelope approximation using an eight-band $\boldsymbol{k \cdot p}$ Hamiltonian. The modified Kane 8×8 Hamiltonian matrix can be given by [11]:

$$H\psi_h(z) = E\psi_h \tag{1}$$

The components of resultant Hamiltonian matrix H=H_0 are:

$$H_0 = \begin{bmatrix} A & 0 & V^* & 0 & \sqrt{3}V & -\sqrt{2}U & -U & \sqrt{2}V^* \\ 0 & A & -\sqrt{2}U & -\sqrt{3}V^* & 0 & -V & \sqrt{2}V & U \\ V & -\sqrt{2}U & -P+Q & -S^* & R & 0 & \sqrt{\frac{3}{2}}S & -\sqrt{2}Q \\ 0 & -\sqrt{3}V & -S & -P-Q & 0 & R & -\sqrt{2}R & \frac{1}{\sqrt{2}}S \\ \sqrt{3}V^* & 0 & R^* & S & -P+Q & S^* & \frac{1}{\sqrt{2}}S^* & \sqrt{2}R^* \\ -\sqrt{2}U & -V^* & 0 & R^* & S & -P+Q & \sqrt{2}Q & \sqrt{\frac{3}{2}}S^* \\ -U & \sqrt{2}V^* & \sqrt{\frac{3}{2}}S^* & -\sqrt{2}R^* & \frac{1}{\sqrt{2}}S & \sqrt{2}Q & -P-\Delta & 0 \\ \sqrt{2}V & U & -\sqrt{2}Q & \frac{1}{\sqrt{2}}S^* & \sqrt{2}R & \sqrt{\frac{3}{2}}S & 0 & -P-\Delta \end{bmatrix} \tag{2}$$

$$\Psi_h(z) = \begin{bmatrix} \Phi_{1/2,1/2}(z) \\ \Phi_{1/2,-1/2}(z) \\ \Phi_{3/2,1/2}(z) \\ \Phi_{3/2,-1/2}(z) \\ \Phi_{3/2,3/2}(z) \\ \Phi_{3/2,-3/2}(z) \\ \Phi_{1/2,1/2}(z) \\ \Phi_{1/2,-1/2}(z) \end{bmatrix} = \begin{bmatrix} g^{(1)}(z) \\ g^{(2)}(z) \\ g^{(3)}(z) \\ g^{(4)}(z) \\ g^{(5)}(z) \\ g^{(6)}(z) \\ g^{(7)}(z) \\ g^{(8)}(z) \end{bmatrix} \tag{3}$$

Where, ϕ_{j,m_j} or $g^{(j)}$ is the conduction and valence band wave function component and E is the energy of conduction band and three valence bands. The atomic Bloch states shown in Table I are Eigen states of the Hamiltonian H_0. Γ_6 corresponds to the conduction band, Γ_8 denotes the heavy-hole (m_j=±3/2) and Γ_8 (m_j=±1/2) the light-hole band. Γ_7 is known as split-off band.

Table I: The atomic basis states at Γ point

u_i	$\lvert j,m_j\rangle$	$\Psi_{j,mj}$	$E_i(k=0)$	
u_1	1/2,1/2	$i\lvert s\uparrow\rangle$	0	Γ_6
u_3	3/2, 1/2	$-\sqrt{(2/3)}\lvert Z\uparrow\rangle + \sqrt{(1/6)}\lvert X+iY\rangle\uparrow\rangle$	$-E_0$	Γ_8
u_5	3/2 ,3/2	$1/\sqrt{2}\lvert X+iY\rangle\uparrow\rangle$	$-E_0$	Γ_8
u_7	1/2,1/2	$\sqrt{(1/3)}\lvert Z\uparrow\rangle + \sqrt{(1/3)}\lvert X+iY\rangle\downarrow\rangle$	$-E_0-\Delta$	Γ_7
u_2	1/2,-1/2	$i\lvert s\downarrow\rangle$	0	Γ_6
u_4	3/2,-1/2	$-\sqrt{(2/3)}\lvert Z\downarrow\rangle - \sqrt{(1/6)}\lvert X-iY\rangle\uparrow\rangle$	$-E_0$	Γ_8
u_6	3/2,-3/2	$1/\sqrt{2}\lvert X-iY\rangle\downarrow\rangle$	$-E_0$	Γ_8
u_8	1/2,-1/2	$\sqrt{(1/3)}\lvert Z\downarrow\rangle - \sqrt{(1/3)}\lvert X-iY\rangle\uparrow\rangle$	$-E_0-\Delta$	Γ_7

The matrix elements are:

$$A = E_c - \frac{\hbar^2}{2m_0}(k_x^2+k_y^2+k_z^2) \tag{4}$$

$$P = -E_v - \gamma_1\frac{\hbar^2}{2m_0}(k_x^2+k_y^2+k_z^2) \tag{5}$$

$$Q = -\gamma_2\frac{\hbar^2}{2m_0}(k_x^2+k_y^2+k_z^2) \tag{6}$$

$$R = \sqrt{3}\frac{\hbar^2}{2m_0}[\gamma_2(k_x^2 - k_y^2) - 2i\gamma_3 k_x k_y] \tag{7}$$

$$S = -\sqrt{3}\gamma_3\frac{\hbar^2}{2m_0}k_z(k_x - ik_y) \tag{8}$$

$$U = \frac{-i}{\sqrt{3}}P_0 k_z \tag{9}$$

$$V = \frac{-i}{\sqrt{6}}P_0(k_x - ik_y) \tag{10}$$

P_0 is the coupling between the conduction and valence bands, E_c and E_v are the (unstrained) conduction and valence band energies respectively, Δ is the spin orbit splitting and γ_i's are modified Luttinger parameters. The energy dispersion profile along (100) orientation is shown as a function of k for the 8-band k.p theory by diagonalizing the Hamiltonian using numerical finite difference scheme.

C. *Crystal orientation dependent wave vector*

If the active channel is grown on (hkl) crystal orientation, the wave vectors on (100) crystal can be anticipated by the following expression [12]:

$$\begin{pmatrix} k_1 \\ k_2 \\ k_3 \end{pmatrix} = O_R \begin{pmatrix} k_x \\ k_y \\ k_z \end{pmatrix} \tag{11}$$

.The expression of the rotation matrix is as follows [13]:

$$O_R = \begin{pmatrix} cos\theta cos\emptyset & -sin\emptyset & sin\theta cos\emptyset \\ cos\theta sin\emptyset & cos\emptyset & sin\theta sin\emptyset \\ -sin\theta & 0 & cos\theta \end{pmatrix}$$

Where, $\theta = \tan^{-1}\left(\frac{\sqrt{(h^2+k^2)}}{l}\right)$ and $\phi = \tan^{-1}(k/h)$

Applying the wave vector in the (100) crystal orientation, the Hamiltonian matrix for (100) crystal orientation can be calculated according to eq. 2. Then the Hamiltonian matrix in (hkl) orientation can be counted by the simple equation:

$$H^{hkl} = U H^{(100)} U^* \tag{12}$$

Where, $U = R(\theta)R(\phi)$

In this formulae, $R(\theta)$ and $R(\phi)$ are denoted as rotations which transform the (100) orientated valence band Hamiltonian to arbitrary crystal orientated Hamiltonian matrix. The argument of $R(\theta)$ and $R(\phi)$ can be defined by:

$$R(\theta) = \begin{pmatrix} \alpha^2 & -\sqrt{3}\alpha^2\zeta & \sqrt{3}\alpha\zeta^2 & \zeta^3 \\ \sqrt{3}\alpha^2\zeta & \alpha^3 - 2\alpha\zeta^2 & -2\alpha^2\zeta + \zeta^3 & \sqrt{3}\alpha\zeta^2 \\ \sqrt{3}\alpha\zeta^2 & 2\alpha^2\zeta - \zeta^3 & \alpha^3 - 2\alpha^2\zeta & -\sqrt{3}\alpha^2\zeta \\ \zeta^3 & \sqrt{3}\alpha\zeta^2 & \sqrt{3}\alpha^2\zeta & \alpha^3 \end{pmatrix} \tag{13}$$

$$\alpha = \cos\frac{\theta}{2} \text{ and } \zeta = -\sin\frac{\theta}{2}$$

$$R(\phi) = \begin{pmatrix} e^{i(3/2)\phi} & 0 & 0 & 0 \\ 0 & e^{i(1/2)\phi} & 0 & 0 \\ 0 & 0 & e^{-i(1/2)\phi} & 0 \\ 0 & 0 & 0 & e^{-i(3/2)\phi} \end{pmatrix} \tag{14}$$

D. *Optical Gain*

The optical gain as a function of energy for quantum well structure can be approximated by [14]:

$$g(E) = \frac{2q^2\hbar}{n\varepsilon_0 c m_0^2 LE}\times\sum_{n,m}\int_0^\infty \frac{k_t M_{nm}(k_t)\Gamma/(2\pi)}{(E_{cn}(k_t) - E_{kpm}(k_t) - E)^2 + (\Gamma/2\pi)^2}(f_c^n - f_v^m)dk_t \tag{15}$$

Here, q is denoted as free electron charge, $\hbar$ as reduced Planck constant, n as the index of refraction, ε_0 as free space dielectric constant, c as speed of light, E as photon energy, E_{cn} as the nth conduction sub-bands, E_{kpm} as the mth valence

sub-bands, and M_{nm} as the momentum matrix element in strained quantum well architecture. $\Gamma = \frac{h}{\tau}$; τ is the photon relaxation time. F_c, F_v are the Fermi levels of conduction and valence band. The momentum matrix element for transition can be written as:

$$M_{nm}(k_t) = \frac{3}{4}\left[\left\langle \Psi_{n(k_t=0)} \middle| g_m{}^{(1)} \right\rangle^2 + \frac{1}{3}\left\langle \Psi_{n(k_t=0)} \middle| g_m{}^{(2)} \right\rangle^2\right] M_b{}^2$$

$$\left\langle \Psi_{n(k_t=0)} \middle| g_m{}^{(1)} \right\rangle = \int_{-\infty}^{\infty} \Psi_{n(k_t=0)}(z) g_m{}^{(1)}(z) dz$$

M_b is the bulk average crystal momentum matrix that can be noted by (E_g=band gap and Δ=split-off band separation):

$$M_b = \left(\frac{m_0}{m_e} - 1\right)\frac{m_0 E_g(E_g+\Delta)}{6(E_g+\frac{2}{3}\Delta)} \quad (16)$$

III. RESULTS AND DISCUSSIONS

Following the k.p method formula given in Section 2, the optical properties of lattice matched 10 nm ZB InP/$In_{0.53}Ga_{0.47}As$ QW VCSEL structure at the Γ-point have been studied. The simulation is carried out in MATLAB environment at room temperature. The valence band dispersion curves obtained in (100), (110), (111), (113) and (131) crystal orientations for the first Brillouin zone have been shown in Fig. 2 (a)-(e) where HH, LH and SH indicate heavy hole, light hole and spin-orbit split off hole bands. To compare the orientation dependent energies, the figures are plotted as a function of wave vector in the same scale. It has been observed, for values of k≠0 (wave vector in the plain direction), the increasing conduction and spin-orbit split off band coupling offer strong anisotropy of the topmost valence band structure at (110) and (111) orientation. Lasing action occurs due to the allowed transition from conduction band (C) to HH. Other transitions such as intra-subbands transitions are forbidden because it reduces the gain of the laser. Among the intra-subbands, transition probability is highest between HH and LH, which is reduced when the energy separation between them is higher. For (111) orientation, larger energy spacing between HH and LH has been observed causing the variation of electron and hole mass m*, which changes the topmost curvature of valence sub-bands as well as emission profile. In order to explain the wavelength dependence of peak emission wavelength the energy separation between the C-HH and HH-LH bands is estimated from the energy band dispersion profiles and listed in table II. It is found that the energy separation between conduction band minima and valence band maxima changes with crystal plane orientations. It can be seen from the table that the intraband mixing effect is minimum for this laser along (111) orientation. With the easy MOVPE growth, the fabrication of (110) oriented VCSEL has strong possibility. The orientation dependent peak gain can be revealed by the momentum matrix elements that depend on the overlapping wave functions of electrons and holes. It is observed from fig. 3 that transition probability is maximum in (111) orientation and least in (113) and (131) orientations. The lowest band gap and minimum intraband interaction is responsible for the improved result along (111). Here we have calculated the optical gain spectra in different crystal orientations using Eq. (15) and shown in Fig. 4 and the approximated gains is found to be 3700, 4650, 4800, 4200 and 3990 cm^{-1} in (100), (110), (111), (113), and (131) orientations, respectively. Here highest gain is observed in (111) crystal orientation and lowest gain is in (100) orientation. The highest gain in (111) crystal orientation is obtained due to the small band mixing effect and greater transition probability. For this similar issue, minimum gain is observed in (100) crystal orientation. The peak emission wavelength are found to be 1.68, 1.55, 1.77, 1.58 and 1.75 μm for (100), (110), (111), (113) and (131) crystal orientations.

That demonstrates peak emission spectra (λ) can be tuned from 1680 to 1770 nm with the change in plane orientation from (100) to (111). The cause of tuning λ is due to the energy gap between C and HH bands. Moreover, an interesting phenomenon is observed in (111) as the C-HH band gap is 0.794 eV which indicates the lasing emission wavelength of 1.55μm that covers minimum chromatic dispersion range of OFC. The crystal orientation-dependent differential gain is calculated and shown in fig.5. The maximum differential gains are obtained when the injected carrier densities 2.75×10^{18} cm^{-3} and 3.0×10^{18} cm^{-3} in (111) and (113) crystal orientations. For (100), (110), and (131) crystal orientations, the maximum differential gains are evaluated when the injection carrier density is $3.25\times10^{18}cm^{-3}$.

So, it is quite visible that (111)-oriented vertical cavity surface emitting InGaAs/InP Laser system leads to have high performance. Also, in (110) oriented growth, the laser emits at 1550nm.

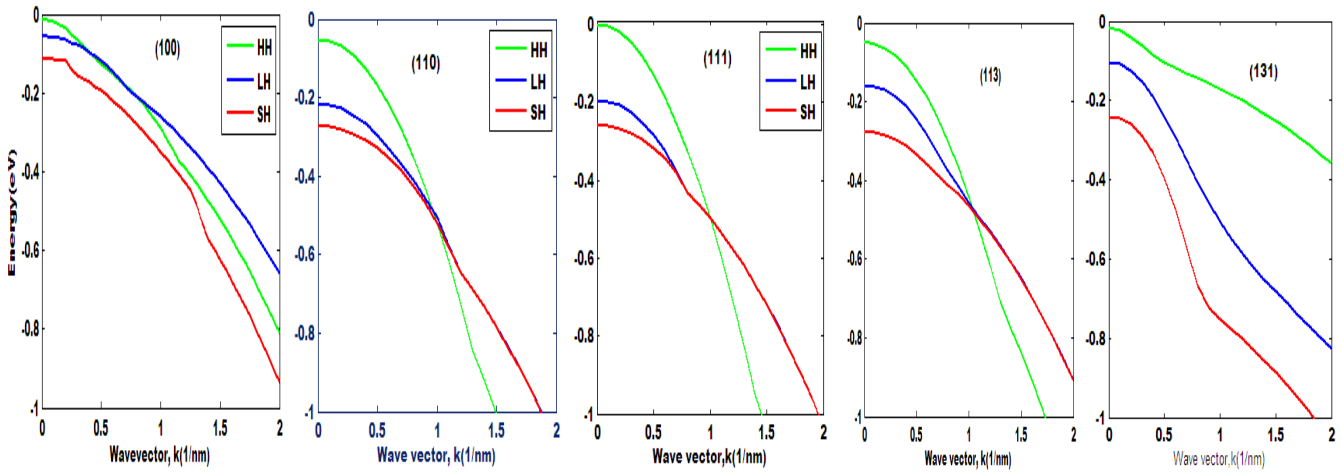

Fig. 2: Valence band dispersion profile of (a) 100 (b) 110 (c) 111 (d) 113 and (e) 131-oriented InGaAs/InP Laser.

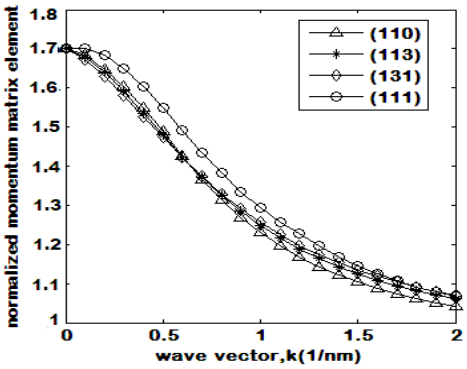

Fig 3. Momentum matrix element in different crystal orientations

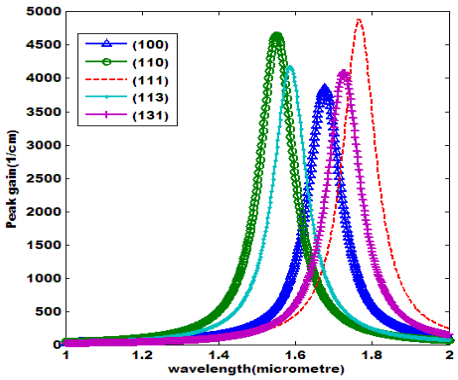

Fig. 4: Orientation dependent optical emission profile

Table I. Orientation dependent energy separation

Crystal orientation	C-HH (eV)	HH-LH (eV)
(100)	0.738	0.03
(110)	0.794	0.17
(111)	0.702	0.20
(113)	0.782	0.10
(131)	0.714	0.07

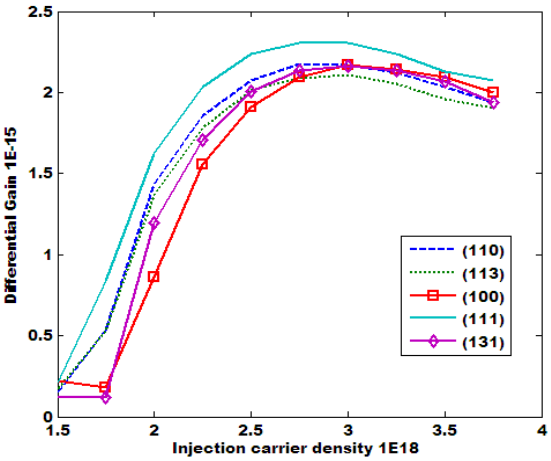

Fig 5: Differential gain in different orientation

IV. Conclusion

To summarize, the influence of crystal orientation on optical properties of Lattice matched zinc-blend InGaAs/InP QW VCSEL are demonstrated at the Γ-point by practicing the eight band *k.p* method including spin orbit coupling. The theoretical results depict the exclusive variation of conduction and valence band energy band dispersion profile with crystallographic direction. Due to minimum interaction from distant band, larger splitting between heavy hole and light hole band is observed in (111) orientation. As the maximum value of momentum matrix element is also evaluated in this orientation, the maximum optical gain is found to be 4800 cm^{-1}. Peak emission wavelength can be tuned from 1680 to 1770 nm with the tuning in crystal orientation from (100) to (111). This result regards that (111) and (110)-oriented InGaAs/InP QW VCSE Laser is a highly potential material for the fabrication of high speed optoelectronic devices in the minimum dispersion range for optical fiber communication.

References

[1] T.Enoki, E.Sano & T.Ishibashi, "Prospects of InP-based IC technologies for 100-Gbit/S –class lightwave communication systems," International Journal of High Speed Electronics and Systems, Vol. 11, No. 1 (2001) pp. 137-158.

[2] R. P. Schneider and J. A. Lott, ''Cavity design for improved electrical injection in InAlGaP/AlGaAs visible (639-661 nm) vertical-cavity surface-emitting laser diodes,'' Applied Physics Letters, vol. 63, no. 7, pp. 917 -919, Sep. 1993.

[3] K.F. Huang, K. Tai, C.C. Wu and J.D. Wynn, ''Continuous wave visible InGaP/InGaAlP quantum-well surface-emitting laser diodes,''IEEE Trans. Electron Devices, vol. 40, no. 11, pp. 613-614, Nov. 1993.

[4] Temkin et al., InGaAs/lnP graded index quantum wen lasers with nearly ideal static characteristics, Applied Physics Letters 56, 1222 (1990).

[5] M. Phon, Y. Chung, W.I. Wang, Orientation dependence of valence subband structures in GaAs-$Ga_{1-x}Al_xAs$ quantum well structures, .Appl. Phys. 64 (1988) pp. 4609-4613.

[6] D.A. Woolf et al. , The homoepitaxial growth of non-axis GaAs (111)A, (111)B and(201) compared with GaAs(100): doping and growth temperature studies,J. Cryst. Growth 127 (2002) 913-917.

[7] R. Notzel, K.H. Ploog, Man-made low-dimensional solids: new challenges inmicrostructure material science, Int. .J. Mod. Phys. B7 (1993), pp. 2743-2778.

[8] Sourav Roy, Nazmus Sakib, Utpal Bhowmik and Md. Rafiqul Islam, "Piezoelectric field-dependent optical properties of InGaAs/GaAs quantum well architecture in arbitrary crystal orientation", 17th International Conference on Computer and Information Technology (ICCIT), 2014, Dhaka, Bangladesh.

[9] Bakin et al., "Simulation of the orientation-dependent growth of InGaAs/InP by MOVPE, Journal of Applied Physics 76, 4906 (1994).

[10] G. Zwinge, H.H. Wehmann, A. Schlachetzki, and C. C. Hsu, "Orientation-dependent growth of InGaAs/InP for applications in laserdiode arrays", Journal of Applied Physics 74, 5516 (1993).

[11] Craig Pryor, Eight-band calculations of strained InAs/GaAs quantum dots compared with one, four, and six-band approximations, Physical Review B, 03/1998.

[12] M.M. Hasan, et al., Crystallographic orientation-dependent optical properties of GaInSb mid-infrared quantum well laser, Optik - Int. J. Light Electron Opt. (2011), doi:10.1016/j.ijleo.2011.09.021

[13] Dragica Vasileska, Tutorial for semiconductor band structure calculation,Arizona State University, Tempe, AZ

[14] A. Niwa, T. Ohtoshi, T. Kuroda, Orientation dependence of optical properties in long wavelength strained quantum-well lasers, IEEE J. Selected Top. Quantum Electron. 1 (1995) 211- 217.